

Modeling incompressible thermal flows using a central-moment-based lattice Boltzmann method

Linlin Fei^a, K. H. Luo^{a,b,*}, Chuandong Lin^a, Qing Li^c

^a Center for Combustion Energy; Key laboratory for Thermal Science and Power Engineering of Ministry of Education, Department of Thermal Engineering, Tsinghua University, Beijing 100084, China

^b Department of Mechanical Engineering, University College London, Torrington Place, London WC1E 7JE, UK

^c School of Energy Science and Engineering, Central South University, Changsha 410083, China

Abstract

In this paper, a central-moment-based lattice Boltzmann (CLB) method for incompressible thermal flows is proposed. In the method, the incompressible Navier-Stokes equations and the convection-diffusion equation for the temperature field are solved separately by two different CLB equations. Through the Chapman-Enskog analysis, the macroscopic governing equations for incompressible thermal flows can be reproduced. For the flow field, the tedious implementation for CLB method is simplified by using the shift matrix with a simplified central-moment set, and the consistent forcing scheme is adopted to incorporate forcing effects. Compared with several D2Q5 multiple-relaxation-time (MRT) lattice Boltzmann methods for the temperature equation, the proposed method is shown to be better Galilean invariant through measuring the thermal diffusivities on a moving reference frame. Thus a higher Mach number can be used for convection flows, which decreases the computational load significantly. Numerical simulations for several typical problems confirm the accuracy, efficiency, and stability of the present method. The grid convergence tests indicate that the proposed CLB method for incompressible thermal flows is of second-order accuracy in space.

Keywords: CLB, incompressible flows, thermal flows

2010 MSC: 00-01, 99-00

1. Introduction

As a mesoscopic numerical method based on the kinetic theory, the lattice Boltzmann method (LBM) [1, 2, 3] has obtained remarkable success in the applications to fluid flows and heat transfer problems during the past three decades [4, 5, 6, 7, 8, 9]. The LBM solves a discretized Boltzmann equation, designed to recover the Navier-Stokes (N-S) equations in the macroscopic limit. The highly efficient and easy algorithm of LBM makes it at affordable computational cost, while the meso-scale nature allows its natural incorporation of micro and/or meso-scale physics [7].

In the standard collision-streaming algorithm for LBM, the simplest collision operator is the single-relaxation-time (SRT) or BGK operator, in which all the distribution functions are relaxed to their local equilibrium values at a common rate [1]. However, the BGK-LBM may meet troubles of inaccuracy in implementing the boundary conditions [10, 11, 12], as well as numerical instability at high Reynolds number or low-viscosity flows [13]. To overcome these difficulties, other collision operators, such as multiple-relaxation-time (MRT) operator [14, 13], entropic operator [15, 16, 17] and two-relaxation-time (TRT) operator [18, 19] have been developed. Recently, a cascaded or central-moment-based operator was proposed by Geier et al. [20]. The collision in the central-moment-based Lattice Boltzmann method (CLBM) is carried out by relaxing central moments of the discrete distribution functions separately, rather than raw moments as in the

*Corresponding author

Email address: K.Luo@ucl.ac.uk (K. H. Luo)

MRT-LBM. By matching the higher order central moments of the continuous Maxwell-Boltzmann distribution naturally, CLBM achieves a higher order of Galilean invariance [20]. Meanwhile, as mentioned by Geier et al. [20], central moments can be expressed as polynomials of raw moments at the same order and below, which means relaxing raw moments (in MRT) affects the independent relaxation for central moments at higher orders. The “cross-talk” is a source of numerical instability, and can be removed through relaxing central moments in CLBM. By setting high-order central moments to their equilibrium values, CLBM has been used to simulate turbulence flow at $Re = 1400000$ using coarse grids without resorting to any turbulence models or entropic stabilization [20]. More recently, CLBM has been extended to multiphase flows based on the interaction potential method [21] by Lycett-Brown and Luo [22]. Compared with the BGK-LBM for multiphase flows, the proposed multiphase CLBM enables significant improvement in reducing spurious currents near the phase interface [22], and achieving higher stability range for the Reynolds number [23]. They further extended the model with an improved forcing scheme [24], and made a breakthrough for large density ratio multiphase flow with high Reynolds and Weber numbers simultaneously [25].

Although CLBM has gained success in high Reynolds number single-phase flows and multiphase flows, its applications are still mainly limited to isothermal flows [26]. The motivation of the present work is to extend CLBM to incompressible thermal flows. Up to now, the double-distribution function (DDF) approach has been extensively used for constructing thermal LBMs [8, 27, 28, 29, 30, 31, 32, 33]. In DDF-based incompressible thermal LBMs, a density or pressure distribution function is used to solve the velocity field, with another distribution for temperature field, where the two fields are usually coupled through the Boussinesq approximation [29, 30]. Due to the simplicity of the convection diffusion equation, a simpler lattice is often used for the temperature field to decrease the computational load and save the memory storage [29, 34]. The MRT operator is also widely used for the temperature field to achieve better numerical stability and more accurate boundary conditions [35, 36, 37]. Inspired by these studies, we try to extend the CLBM to incompressible thermal flows in the present study based on the DDF approach. Specifically, a density distribution function and a temperature distribution function are used to simulate the velocity field and the temperature field, respectively, and both of them are relaxed using the central-moment-based operator.

The rest of the paper is structured as follows: In Section 2, the 2D CLBM for incompressible thermal flows is presented in detail. Numerical experiments are carried out for several benchmark problems to validate the proposed method in Section 3. Finally, concluding remarks are given in Section 4.

2. CLBM for incompressible thermal flows

In this section, details for the construction of the CLBM for incompressible thermal flows are given. The macroscopic governing equations for the flow fields are

$$\nabla \cdot \mathbf{u} = 0, \quad (1a)$$

$$\frac{\partial \mathbf{u}}{\partial t} + \mathbf{u} \cdot \nabla \mathbf{u} = -\frac{1}{\rho_0} \nabla p + \nu \nabla^2 \mathbf{u} + \mathbf{F}, \quad (1b)$$

where \mathbf{u} , p , ρ_0 , \mathbf{F} and ν are the velocity, pressure, reference density, force field and kinematic viscosity, respectively. The convection-diffusion equation for a scalar variable ϕ with diffusion coefficient D can be written as

$$\frac{\partial \phi}{\partial t} + \mathbf{u} \cdot \nabla \phi = \nabla \cdot (D \nabla \phi). \quad (2)$$

For the incompressible thermal flows considered in this study, the scalar variable and diffusion coefficient are specified as temperature T and thermal diffusivity α , respectively. To include the effect of temperature field on the flow field, the Boussinesq assumption is used and the force field is defined by

$$\mathbf{F} = -\mathbf{g}\beta(T - T_0) + \mathbf{F}_v, \quad (3)$$

where the gravitational acceleration vector \mathbf{g} points to the negative direction of y-axis, β is the thermal expansion coefficient, T_0 is the reference temperature, and \mathbf{F}_v is an external body force.

The two-dimensional (2D) problems are considered in this study, and the D2Q9 lattice [1] is used for the flow field. The lattice speed $c = \Delta x / \Delta t = 1$ is adopted, in which Δx and Δt are the lattice spacing and time step. The discrete velocities $\mathbf{e}_i = [|e_{ix}\rangle, |e_{iy}\rangle]$ are defined by

$$|e_{ix}\rangle = [0, 1, 0, -1, 0, 1, -1, -1, 1]^\top, \quad (4a)$$

$$|e_{iy}\rangle = [0, 0, 1, 0, -1, 1, 1, -1, -1]^\top, \quad (4b)$$

where $i = 0 \dots 8$, $|\cdot\rangle$ indicates the column vector, and the superscript \top indicates the transposition.

To construct the central-moment-based collision operator, raw moments and central moments for the discretized distribution functions (DFs) f_i are introduced,

$$k_{mn} = \langle f_i | e_{ix}^m e_{iy}^n \rangle, \quad (5a)$$

$$\tilde{k}_{mn} = \langle f_i | (e_{ix} - u_x)^m (e_{iy} - u_y)^n \rangle, \quad (5b)$$

and the equilibrium values k^{eq} and \tilde{k}^{eq} are defined analogously by replacing f_i with the discrete equilibrium distribution functions (EDFs) f_i^{eq} . In the literature, many researchers [20, 22, 23, 25, 26, 38, 39] using the recombined raw moments $k_{20} + k_{02}, k_{20} - k_{02}$, to treat the trace of the pressure tensor and the normal stress difference independently. To simplify the tedious implementation of using the recombined raw-moment set, a simplified method was proposed in [40], where the raw moments k_{20}, k_{02} were used and some modifications were made in the relaxation matrix. In this work, the simplified raw-moment set is adopted,

$$|\Gamma_i\rangle = [k_{00}, k_{10}, k_{01}, k_{20}, k_{02}, k_{11}, k_{21}, k_{12}, k_{22}]^\top, \quad (6)$$

and so do the recombined central moments $\tilde{\Gamma}_i$. To be more specific, the raw moments can be given from f_i through a transformation matrix \mathbf{M} by $|\Gamma_i\rangle = \mathbf{M} |f_i\rangle$, and the central moments shifted from raw moments can be realized through a shift matrix \mathbf{N} by $|\tilde{\Gamma}_i\rangle = \mathbf{N} |\Gamma_i\rangle$. Similar to the expressions in [38], \mathbf{M} and \mathbf{N} are written as,

$$\mathbf{M} = \begin{bmatrix} 1 & 1 & 1 & 1 & 1 & 1 & 1 & 1 & 1 \\ 0 & 1 & 0 & -1 & 0 & 1 & -1 & -1 & 1 \\ 0 & 0 & 1 & 0 & -1 & 1 & 1 & -1 & -1 \\ 0 & 1 & 0 & 1 & 0 & 1 & 1 & 1 & 1 \\ 0 & 0 & 1 & 0 & 1 & 1 & 1 & 1 & 1 \\ 0 & 0 & 0 & 0 & 0 & 1 & -1 & 1 & -1 \\ 0 & 0 & 0 & 0 & 0 & 1 & 1 & -1 & -1 \\ 0 & 0 & 0 & 0 & 0 & 1 & -1 & -1 & 1 \\ 0 & 0 & 0 & 0 & 0 & 1 & 1 & 1 & 1 \end{bmatrix}, \quad (7a)$$

$$\mathbf{N} = \begin{bmatrix} 1 & 0 & 0 & 0 & 0 & 0 & 0 & 0 & 0 & 0 \\ -u_x & 1 & 0 & 0 & 0 & 0 & 0 & 0 & 0 & 0 \\ -u_y & 0 & 1 & 0 & 0 & 0 & 0 & 0 & 0 & 0 \\ u_x^2 & -2u_x & 0 & 1 & 0 & 0 & 0 & 0 & 0 & 0 \\ u_y^2 & 0 & 2u_y & 0 & 1 & 0 & 0 & 0 & 0 & 0 \\ u_x u_y & -u_y & -u_x & 0 & 0 & 1 & 0 & 0 & 0 & 0 \\ -u_x^2 u_y & 2u_x u_y & u_x^2 & -u_y & 0 & -2u_x & 1 & 0 & 0 & 0 \\ -u_y^2 u_x & u_y^2 & 2u_x u_y & 0 & -u_x & -2u_y & 0 & 1 & 0 & 0 \\ u_x^2 u_y^2 & -2u_x u_y^2 & -2u_y u_x^2 & u_y^2 & u_x^2 & 4u_x u_y & -2u_y & -2u_x & 1 & 0 \end{bmatrix}. \quad (7b)$$

By relaxing each central moment to its equilibrium counterpart independently, the post-collision central moments are given by

$$|\tilde{\Gamma}_i^*\rangle = (\mathbf{I} - \mathbf{S}) |\tilde{\Gamma}_i\rangle + \mathbf{S} |\tilde{\Gamma}_i^{eq}\rangle + (\mathbf{I} - \mathbf{S}/2) |C_i\rangle, \quad (8)$$

where C_i are the forcing source terms in central moments space, and the block-diagonal relation matrix is given by,

$$\mathbf{S} = \text{diag} \left([0, 0, 0], \begin{bmatrix} s_+, s_- \\ s_-, s_+ \end{bmatrix}, [s_\nu, s_3, s_3, s_4] \right), \quad (9)$$

with $s_+ = (s_b + s_\nu)/2$ and $s_- = (s_b - s_\nu)/2$. The equilibrium central moments of the f_i^{eq} are set equal to the continuous central moments of the Maxwellian-Boltzmann distribution in continuous velocity space,

$$|\tilde{\Gamma}_i^{eq}\rangle = [\rho, 0, 0, \rho c_s^2, \rho c_s^2, 0, 0, 0, \rho c_s^4]^\top, \quad (10)$$

where ρ is the fluid density, and $c_s = \sqrt{1/3}$ is the lattice sound speed. The corresponding EDF is in fact a generalized local equilibrium [40, 39]. Consistently, the forcing source terms in central moments space are given by [38],

$$|C_i\rangle = \mathbf{NM} |R_i\rangle = [0, F_x, F_y, 0, 0, 0, c_s^2 F_y, c_s^2 F_x, 0]^\top. \quad (11)$$

In the streaming step, the post-collision discrete DFs in space \mathbf{x} and time t stream to their neighbors in the next time step as usual

$$f_i(\mathbf{x} + \mathbf{e}_i \Delta t, t + \Delta t) = f_i^*(\mathbf{x}, t), \quad (12)$$

where the post-collision discrete DFs are determined by $|f_i^*\rangle = \mathbf{M}^{-1} \mathbf{N}^{-1} |\tilde{\Gamma}_i^*\rangle$. Using the Chapman-Enskog analysis, the incompressible N-S equations in Eq. (1) can be reproduced in the low-Mach number limit [39]. The hydrodynamics variables are obtained by,

$$\rho = \sum_i f_i, \quad \rho \mathbf{u} = \sum_i f_i \mathbf{e}_i + \frac{\Delta t}{2} \mathbf{F}. \quad (13)$$

The kinematic and bulk viscosities are related to the relaxation parameters by $\nu = (1/s_\nu - 0.5)c_s^2 \Delta t$ and $\xi = (1/s_b - 0.5)c_s^2 \Delta t$, respectively.

2.2. CLBM for the temperature field

A new D2Q5 (the five discrete velocity set is defined in Eq. (4), $\{\mathbf{e}_i = [|e_{ix}\rangle, |e_{iy}\rangle] | i = 0, 1, \dots, 4\}$) CLBM is proposed to solve the convection-diffusion equation for the temperature field. Similarly, the raw moments and central moments of the temperature distribution functions g_i can be defined by

$$k_{mn}^T = \langle g_i | e_{ix}^m e_{iy}^n \rangle, \quad (14a)$$

$$\tilde{k}_{mn}^T = \langle g_i | (e_{ix} - u_x)^m (e_{iy} - u_y)^n \rangle. \quad (14b)$$

In the D2Q5 lattice, the following five raw moments are considered,

$$|\Gamma_i^T\rangle = [k_{00}^T, k_{10}^T, k_{01}^T, k_{20}^T, k_{02}^T]^\top, \quad (15)$$

and so do the recombined central moments $|\tilde{\Gamma}_i^T\rangle$. Analogously, the raw moments and central moments can be calculated through a transformation matrix \mathbf{M}_T and a shift matrix \mathbf{N}_T , respectively

$$|\Gamma_i^T\rangle = \mathbf{M}_T |g_i\rangle, \quad |\tilde{\Gamma}_i^T\rangle = \mathbf{N}_T |\Gamma_i^T\rangle. \quad (16)$$

Explicitly, the transformation matrix \mathbf{M}_T is expressed as

$$\mathbf{M}_T = \begin{bmatrix} 1 & 1 & 1 & 1 & 1 \\ 0 & 1 & 0 & -1 & 0 \\ 0 & 0 & 1 & 0 & -1 \\ 0 & 1 & 0 & 1 & 0 \\ 0 & 0 & 1 & 0 & 1 \end{bmatrix}, \quad (17)$$

and the shift matrix $\mathbf{N}_{\mathbf{T}}$ is given by

$$\mathbf{N}_{\mathbf{T}} = \begin{bmatrix} 1 & 0 & 0 & 0 & 0 \\ -u_x & 1 & 0 & 0 & 0 \\ -u_y & 0 & 1 & 0 & 0 \\ u_x^2 & -2u_x & 0 & 1 & 0 \\ u_y^2 & 0 & -2u_y & 0 & 1 \end{bmatrix}. \quad (18)$$

The collision in central moments can also be written as

$$\left| \tilde{\Gamma}_i^{T,*} \right\rangle = (\mathbf{I} - \mathbf{S}_{\mathbf{T}}) \left| \tilde{\Gamma}_i^T \right\rangle + \mathbf{S}_{\mathbf{T}} \left| \tilde{\Gamma}_i^{T,eq} \right\rangle, \quad (19)$$

where $\mathbf{S}^{\mathbf{T}} = \text{diag}(\lambda_0, \lambda_1, \lambda_1, \lambda_2, \lambda_2)$ is the diagonal relaxation matrix. The equilibrium values of the central moments are given by

$$\left| \tilde{\Gamma}_i^{T,eq} \right\rangle = [T, 0, 0, Tc_{T,s}^2, Tc_{T,s}^2]^\top, \quad (20)$$

where $c_{T,s}^2$ is the sound speed in the D2Q5 lattice. The post-collision temperature distribution functions g_i^* can be obtained by

$$g_i^* = \mathbf{M}_{\mathbf{T}}^{-1} \mathbf{N}_{\mathbf{T}}^{-1} \left| \tilde{\Gamma}_i^{T,*} \right\rangle. \quad (21)$$

The streaming step for g_i^* are also as usual

$$g_i(\mathbf{x} + \mathbf{e}_i \Delta t, t + \Delta t) = g_i^*(\mathbf{x}, t). \quad (22)$$

The temperature T is computed as

$$T = \sum_{i=0}^4 g_i. \quad (23)$$

As shown in Appendix A, the convection-diffusion Eq. (2) can be recovered by the D2Q5 CLBM presented in this subsection, and the thermal diffusivity is related to the relaxation parameter by $\alpha = (1/\lambda_1 - 0.5)c_{T,s}^2 \Delta t$.

3. Numerical experiments

In this section, we conduct several benchmark cases to verify the effectiveness and accuracy of the proposed CLBM for incompressible thermal flows. Unless otherwise specified, the lattice sound speed for the D2Q5 CLBM is set to $c_{sT} = 1/2$, the tunable relaxation parameters for high-order central moments are set to 1.0, and the non-equilibrium bounce-back method [41] and non-equilibrium extrapolation method [42] are adopted for velocity and temperature boundary conditions in simulations, respectively.

3.1. The decay of a temperature wave

Firstly, the decay of a temperature wave on a moving frame is considered. The problem is specified by the following velocity and temperature fields:

$$\mathbf{u} = [0, A]. \quad (24a)$$

$$T = T_0 + B \sin[\phi(y - At)] \exp(-\phi^2 \alpha t). \quad (24b)$$

where $\phi = 2\pi/L$, A represents the vertical reference velocity component, and B is the initial amplitude of the temperature wave. Periodic boundary conditions are used along the x and y axes. In the simulations, $T_0 = 1.0$, $L = 100$, and the initial amplitude is set to $B = 0.01$. The velocity field is given, thus only the D2Q5 CLBM is adopted to solve the temperature field. Another two D2Q5 MRT LBMs in [36] and [37] are also used for comparison, and they are denoted by MRT-LBM1 and MRT-LBM2, respectively. Firstly, the case at Mach number $\text{Ma} = A/c_s = 0.3$ is considered. The profiles for the dimensionless temperature T^* in different methods at the time $t^* = 2.0$ are shown in Fig. 1, where $T^* = (T - T_0)/B$ and $t^* = \phi^2 \alpha t$.

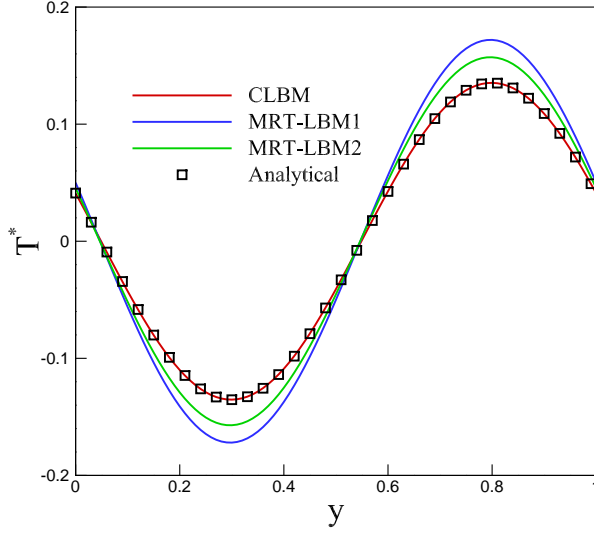


Figure 1: Comparison of the temperature profiles at $t^* = 2.0$ simulated by different methods.

It is found that the simulation result of the present CLBM is in good agreement of the analytical solution, while there are visible differences between the analytical solution and numerical solutions by the other two methods. The measured thermal diffusivity of the simulated fluid is obtained by measuring the time decay of the temperature wave. Then, the measured thermal diffusivities of each method at different values of the Mach number are compared in Fig. 2, while the originally given thermal diffusivity is $\alpha = 0.05$. For the

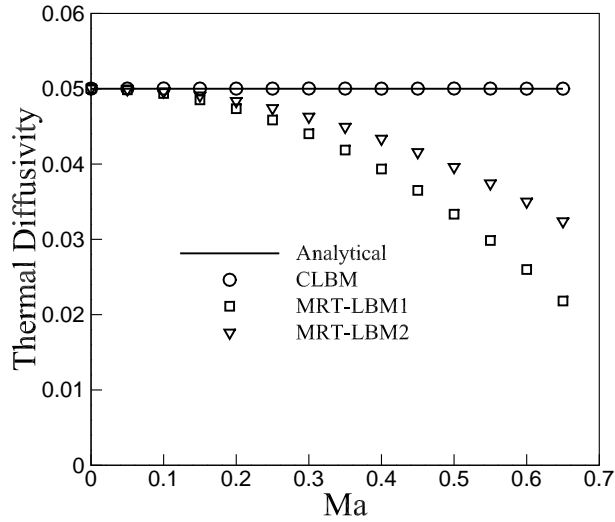


Figure 2: Comparison of the measured thermal diffusivities of each method at different values of Ma .

present D2Q5 CLBM, the measured thermal diffusivity is independent of the reference velocity (or Ma) and always agrees with the given value. For the other two D2Q5 MRT LBMs, the measured diffusivities decrease with the increase of the reference velocity. To be specific, the relative errors at $Ma = 0.3$ are around 12% and 8% for MRT-LBM1 and MRT-LBM2, respectively.

80 3.2. Normal plate velocity problem with a temperature difference

The normal plate velocity problem is a fully developed channel flow, where the upper plate moves with a uniform velocity u_0 , and a uniform normal flow with velocity v_0 is injected through the bottom plate and withdrawn from the upper plate. The analytical solution of the flow is given by [43],

$$\frac{u_a}{u_0} = \frac{\exp(Re \cdot y/L) - 1}{\exp(Re) - 1}, \quad (25)$$

where the Reynolds number is based on the width of the channel, L , and defined by $Re = v_0 L / \nu$. For the present study, a temperature difference $\Delta T = T_H - T_L$ is considered, where T_H and T_L are the temperatures at upper hot plate and bottom cold plate, respectively. The steady temperature profile satisfies [29],

$$\frac{T_a - T_L}{\Delta T} = \frac{\exp(RePr \cdot y/L) - 1}{\exp(RePr) - 1}, \quad (26)$$

where $Pr = \nu / \alpha$ is the Prandtl number.

In the simulations, $T_H = 1.0$ and $T_L = 0$ are used, and the viscosity is set to $\nu = 0.1$. Firstly, we set the Reynolds number $Re = 10$, $u_0 = v_0 = Re\nu/L$ with $L = 50$. Periodic boundary conditions are adopted at the inlet and outlet of channel, and the length of the channel is covered by 5 grids to save the computational cost. Three simulation cases with $Pr = [0.1, 1, 10]$ are conducted to verify the numerical performance of the present method at a wide range of the Prandtl number. The tunable parameter λ_2 is set according to the zero-numerical-slip condition [37], $\lambda_2 = 12(\lambda_1 - 2) / (\lambda_1 - 12)$. The residual error $E_R < 1 \times 10^{-9}$ is used as

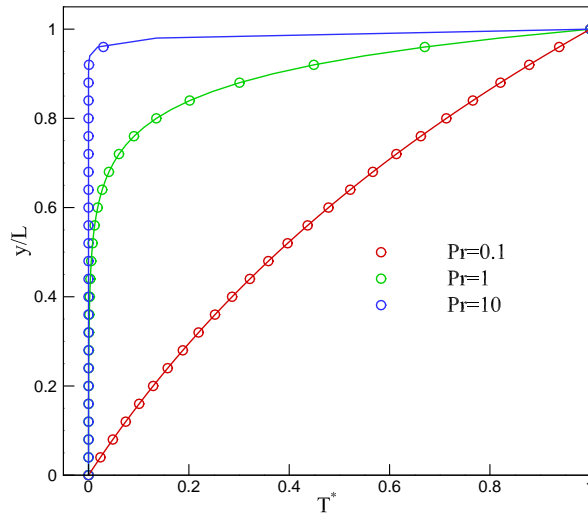


Figure 3: Comparison of numerical temperature profiles (symbols) and the analytical solutions (solid lines) at different values of the Pr .

the convergent criterion, the definition of E_R can be seen in [38]. As shown in Fig. 3, the numerical results for the non-dimensional temperature $T^* = (T - T_0) / \Delta T$ agree very well with the analytical solutions.

Then we set the Prandtl number corresponding to air, $Pr = 0.71$, with different values of the Reynolds number, $Re = [10, 20, 30]$. The width of the channel covered by a series of grid nodes, $L = [30, 60, 90, 120, 150]$, are considered to validate the convergence rate in space. The relative errors of temperature and velocity are calculated according to the following definitions,

$$E_T = \sqrt{\frac{\sum (T - T_a)^2}{\sum T_a^2}}, \quad E_u = \sqrt{\frac{\sum (u - u_a)^2}{\sum u_a^2}}. \quad (27)$$

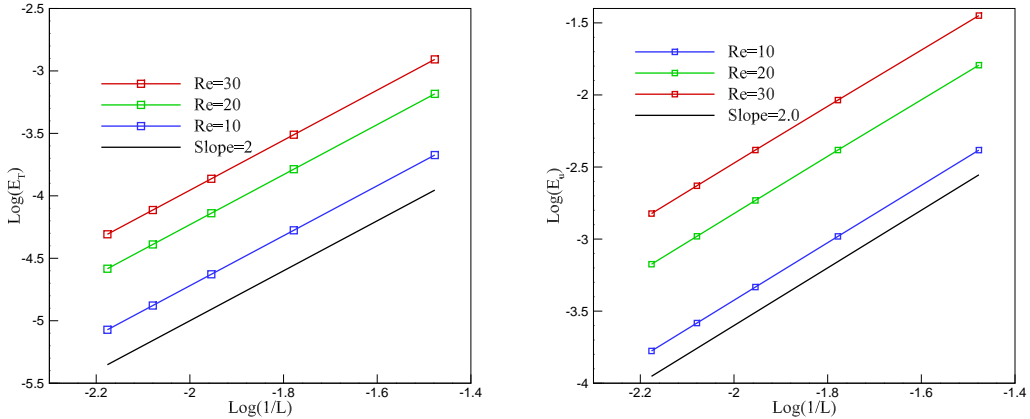


Figure 4: Relative errors of temperature (left) and velocity (right) change with lattice spacings at $Pr = 0.71$ and $Re = [10, 20, 30]$.

90 The relationships between grid size and relative errors of the present method are plotted in Fig. 4, and the slopes of each fitting lines are very close to 2.0. This demonstrates that the method proposed is of second-order convergence rate in space.

3.3. Rayleigh-Bénard convection

In this section, the Rayleigh-Bénard convective flow is conducted to check the ability of simulating incompressible thermal flows with an external force field. In the 2D Rayleigh-Bénard convective flow, the fluid is enclosed between two parallel stationary walls, with high temperature T_H at the bottom and low temperature T_L at the top, and experiences the gravity. The gravity field is incorporated by Eq. (3).

The flow is characterized by the length-width ratio of the flow domain $L : H$, the Prandtl number $Pr = \nu/\alpha$ and Rayleigh number $Ra = g\beta\Delta TH^3/(\nu\alpha)$. In the simulations, we set $L \times H = 60 \times 30$, $Pr = 0.71$, $T_H = 1.05$, $T_L = 0.95$, and $T_0 = (T_H + T_L)/2 = 1.0$. The characteristic velocity of the convection is $u_c = \sqrt{g\beta\Delta TH}$, by which the Mach number is defined, $Ma = u_c/c_s$. For a given Rayleigh number, the viscosity is calculated according to $\nu = Mac_s H \sqrt{Pr/Ra}$. To set up the simulation, a initial small disturbance is given to the density field along the horizontal center line,

$$\rho(x, H/2) = \rho_0 [1.0 + 0.001 \cos(2\pi x/L)], \quad (28)$$

where $\rho_0 = 1.0$, while other points are initialized as ρ_0 .

100 The characteristic time of the system can be expressed by $t_c \sim H/u_c = Hc_s/Ma$. It is known that the iterations needed for the convergence are proportional to t_c . Firstly, we change $1/Ma$ from 0.1 to 0.31 with a 0.03 interval, and calculate the needed time steps until convergence. From Fig. 5, we certainly confirm the linear relation between the needed time steps and $1/Ma$. Throughout the variation range of Ma , the relative changes of the Nusselt number (defined in Eq. 29) are only 0.11%, 0.10% and 0.08% for the Rayleigh numbers at 2500, 3000, and 5000, respectively. Based on this, a higher Mach number can be used in the present method to reduce the computational cost, but not affects the numerical accuracy. In the following simulations, the Mach number is set to $Ma = 0.3$.

110 According to the linear stability theory, the driven force by the density variations induced by the temperature variations will be balanced by the viscous force when Rayleigh number is lower than a critical value Ra_c , while if the Rayleigh number is increased above the threshold, the driving force will dominate and convection will be induced. To determine the critical Rayleigh number, we measure the evolution of the maximum vertical velocity in the system V_{\max} for a series of Rayleigh numbers, $Ra = [1702, 1704, 1706, 1708, 1710]$. It can be seen in Fig 6 that V_{\max} will keep increasing/decreasing approximately linearly in the early period, depending on Ra . The critical Rayleigh number is determined by solving zero value for the grow rate

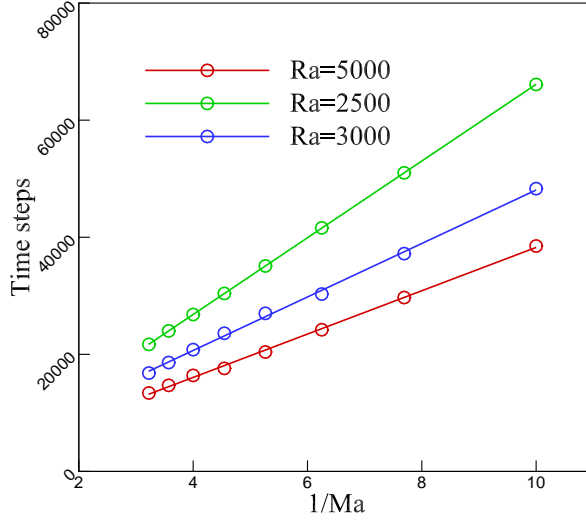


Figure 5: Time steps needed for convergence change with the reciprocal of Ma .

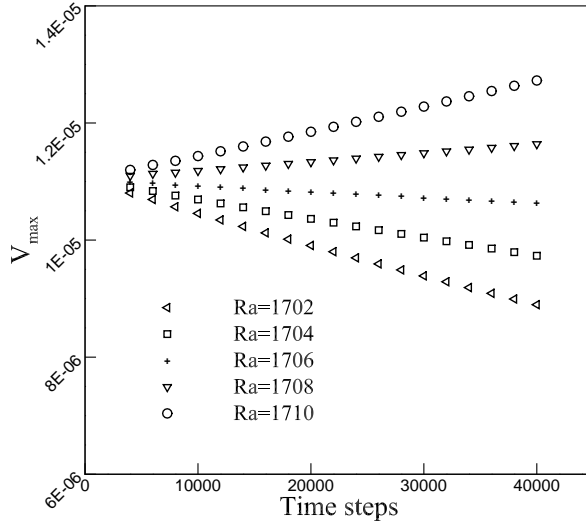


Figure 6: The evolution of V_{\max} with time at $Ra = [1702, 1704, 1706, 1708, 1710]$.

of V_{\max} with the least-square method [35]. Compared with the exact value in the linear stability theory, $Ra_c = 1707.76$, the value based on our method, 1706.82, is satisfying.

Flows at different Rayleigh numbers are then simulated. Figs. 7 display the normalized temperature $(T - T_0) / \Delta T$ at $Ra = 2000, 10000$ and 50000 . When the Rayleigh number increases, we can see two clear trends in the figures: the mixing of the hot and cold fluids is enhanced, and the temperature gradients near the bottom and top walls are increased, both of which mean the convective heat transfer is enhanced in the domain. In the meantime, as shown in Figs. 8, the vortex is gradually distorted with the increase of the Rayleigh number, which also means the enhancement of convection. To quantify this, the Nusselt number in the system is calculated,

$$Nu = 1 + \frac{\langle u_y T \rangle H}{\alpha \Delta T}, \quad (29)$$

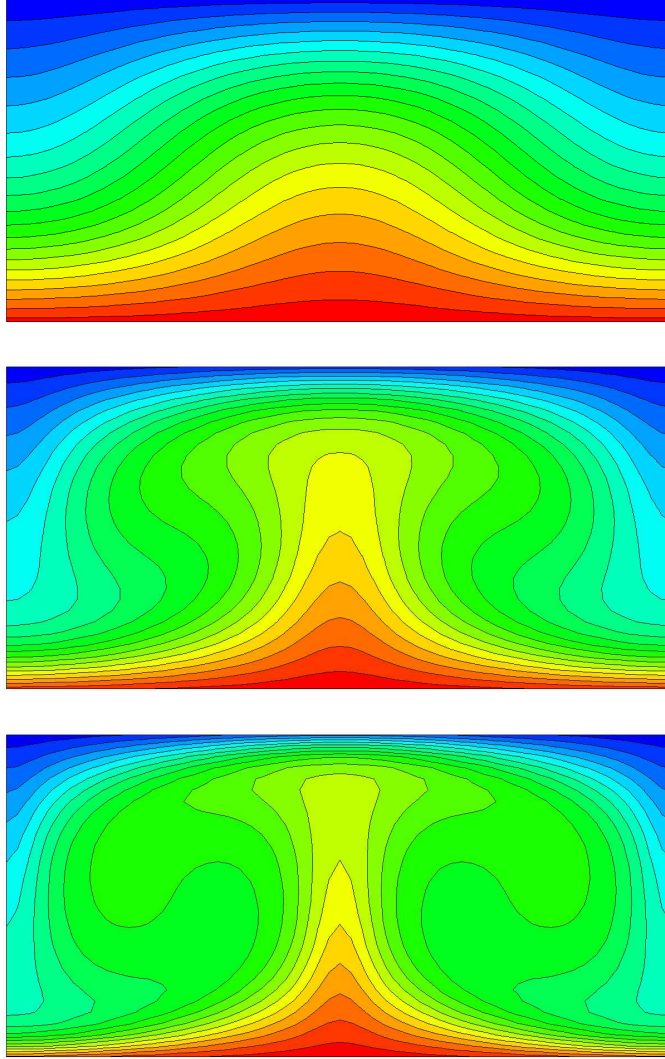


Figure 7: Isotherms for Rayleigh-Bénard convective flows. From top to bottom, $Ra = 2000$, 10000 and 50000 .

where the square bracket represents the average over the whole system. Nusselt numbers obtained at various Rayleigh numbers are compared with the reference data in Table 1. The simulation results are in good agreement with the analytical values in Ref.[44]. On the whole, the relative errors for the present method are smaller than the method in [45], while only 30 nodes are used in the present method rather than 50 nodes as in [45].

120

In the end, it is interesting to find that the proposed method is stable for Ra reaching up to 10^9 with only 220 nodes in the vertical direction as shown in Fig .9, which confirms the commendable stability of the method. However, the study of high-Rayleigh-number thermal convection is beyond the scope of the current paper.

4. Conclusions

In this paper, we have developed a central-moment-based lattice Boltzmann (CLB) model for simulation of incompressible thermal flows. Combined with the D2Q9 CLB equation for the flow field, another D2Q5

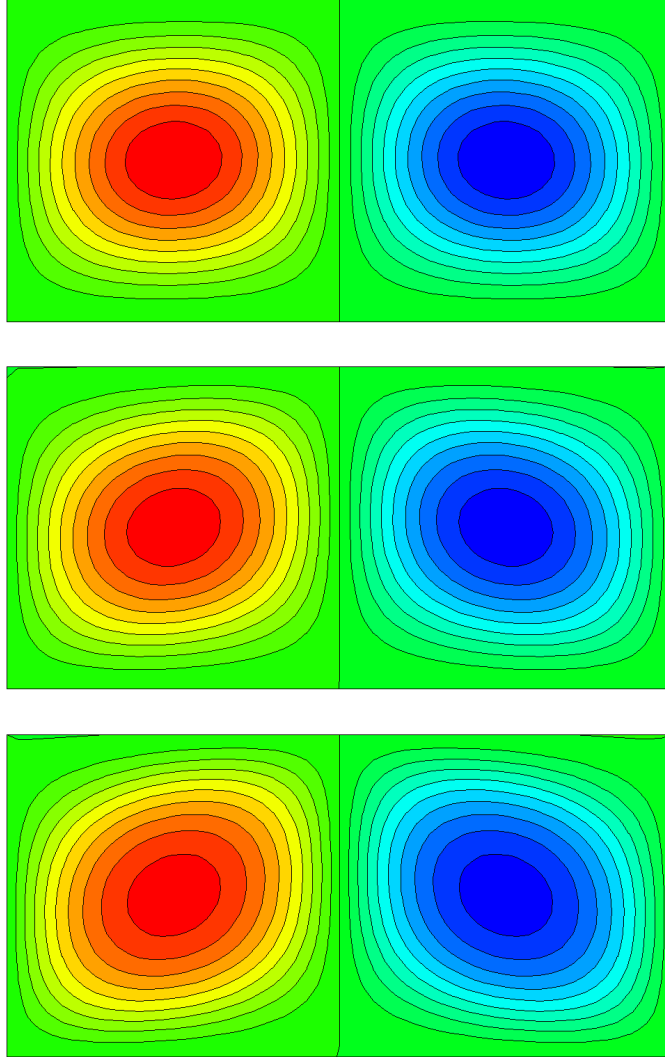


Figure 8: Streamlines for Rayleigh-Bénard convective flows. From top to bottom, $Ra = 2000, 10000$ and 50000 .

CLB equation is designed to reproduce the temperature equation. Through the Chapman-Enskog analysis, the macroscopic governing equations for incompressible thermal flows can be recovered. By matching the higher order central moments of continuous Maxwell-Boltzmann distribution naturally, the proposed thermal model achieves better Galilean invariance compared with some existing thermal LBMs. Thus a higher Mach number can be adopted for convection flows in the present model, which reduces the computational cost significantly. Through the simulation of several canonical problems, the accuracy, efficiency, stability and the second-order convergence rate in space for the present model are verified. The method developed retains the simplicity and numerical efficiency of the standard LBM. In principle, the method can be extended to three-dimensional readily. Besides, the model developed can also be applied to other convection-diffusion problems directly.

Table 1: Comparison of Nusselt number between the present numerical results and the results in Ref. [44, 45].

Cases	Analytic N_u [44]	Present method		Results in Ref. [45]	
		N_u	Relative error	N_u	Relative error
2000	1.212	1.213	0.08	-	-
2500	1.475	1.477	0.13	1.474	0.07
3000	1.663	1.667	0.24	-	-
5000	2.116	2.121	0.24	2.104	0.57
10000	2.661	2.672	0.41	2.664	0.64
20000	3.258	3.271	0.4	-	-
30000	3.662	3.668	0.16	3.605	1.56
50000	4.245	4.229	0.38	4.133	2.64

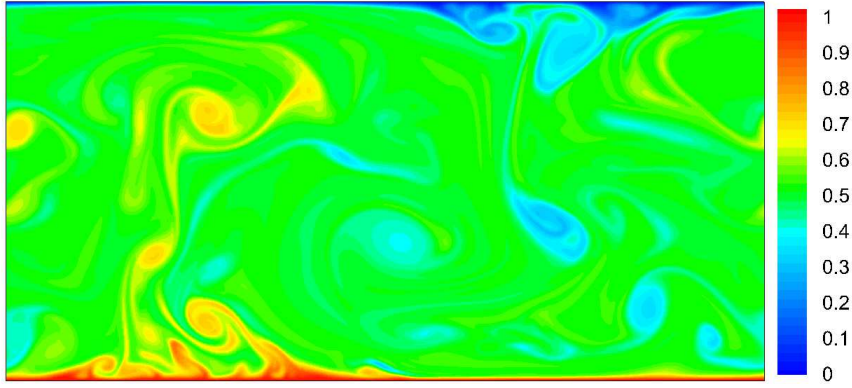


Figure 9: Snapshot of the temperature field at $Ra = 10^9$.

Acknowledgments

Support from the MOST National Key Research and Development Programme (Project No. 2016YFB0600805) and the Center for Combustion Energy at Tsinghua University is gratefully acknowledged. The simulations were partly performed on the Tsinghua High-Performance Parallel Computer supported by the Tsinghua National Laboratory for Information Science and Technology and partly on ARCHER funded under the EPSRC project “UK Consortium on Mesoscale Engineering Sciences (UKCOMES)” (Grant No. EP/L00030X/1).

Appendix A. Chapman-Enskog analysis of the CLBM for temperature field

The explicit expressions for \mathbf{M}_T^{-1} and \mathbf{N}_T^{-1} are as follows.

$$\mathbf{M}_T^{-1} = \begin{bmatrix} 1 & 0 & 0 & -1 & -1 \\ 0 & 1/2 & 0 & 1/2 & 0 \\ 0 & 0 & 1/2 & 0 & 1/2 \\ 0 & -1/2 & 0 & 1/2 & 0 \\ 0 & 0 & -1/2 & 0 & 1/2 \end{bmatrix}, \quad (30)$$

$$\mathbf{N}_{\mathbf{T}}^{-1} = \begin{bmatrix} 1 & 0 & 0 & 0 & 0 \\ u_x & 1 & 0 & 0 & 0 \\ u_y & 0 & 1 & 0 & 0 \\ u_x^2 & 2u_x & 0 & 1 & 0 \\ u_y^2 & 0 & 2u_y & 0 & 1 \end{bmatrix}. \quad (31)$$

The collision step in Eq. (19) and streaming step in Eq. (22) and can be integrated into one step as,

$$g_i(\mathbf{x} + \mathbf{e}_i \Delta t, t + \Delta t) - g_i(\mathbf{x}, t) = -\mathbf{M}_{\mathbf{T}}^{-1} \mathbf{N}_{\mathbf{T}}^{-1} \mathbf{S}_{\mathbf{T}} \mathbf{N}_{\mathbf{T}} \mathbf{M}_{\mathbf{T}} |g_i - g_i^{eq}\rangle. \quad (32)$$

According to the Chapman-Enskog expansion, the following multiscale expansions are usually introduced,

$$g_i(\mathbf{x} + \mathbf{e}_i \Delta t, t + \Delta t) = \sum_{n=0}^{\infty} \frac{\varepsilon^n}{n!} (\partial_t + \mathbf{e}_i \cdot \nabla)^n g_i(\mathbf{x}, t), \quad (33a)$$

$$g_i = g_i^{(0)} + \varepsilon g_i^{(1)} + \varepsilon^2 g_i^{(2)} + \dots, \quad \partial_t = \varepsilon \partial_{t1} + \varepsilon^2 \partial_{t2}, \quad \nabla = \varepsilon \nabla_i, \quad (33b)$$

where ε is the expansion parameter. Using these expansions, the D2Q5 CLBM in Eq. (32) can be written in the consecutive orders of ε ,

$$O(\varepsilon^0) : g_i^{(0)} = g_i^{eq}, \quad (34a)$$

$$O(\varepsilon^1) : (\partial_{t1} + \mathbf{e}_i \cdot \nabla_1) g_i^{(0)} = -\frac{1}{\Delta t} \mathbf{M}_{\mathbf{T}}^{-1} \mathbf{N}_{\mathbf{T}}^{-1} \mathbf{S}_{\mathbf{T}} \mathbf{N}_{\mathbf{T}} \mathbf{M}_{\mathbf{T}} |g_i^{(1)}\rangle, \quad (34b)$$

$$O(\varepsilon^2) : \partial_{t2} g_i^{(0)} + (\partial_{t1} + \mathbf{e}_i \cdot \nabla_1) g_i^{(1)} + \frac{\Delta t}{2} (\partial_{t1} + \mathbf{e}_i \cdot \nabla_1)^2 g_i^{(0)} = -\frac{1}{\Delta t} \mathbf{M}_{\mathbf{T}}^{-1} \mathbf{N}_{\mathbf{T}}^{-1} \mathbf{S}_{\mathbf{T}} \mathbf{N}_{\mathbf{T}} \mathbf{M}_{\mathbf{T}} |g_i^{(2)}\rangle. \quad (34c)$$

If we multiply the matrix $\mathbf{M}_{\mathbf{T}}$ on both sides of Eqs. (34), the corresponding equations in the raw moment can be rewritten as,

$$O(\varepsilon^0) : \Gamma_i^{T,(0)} = \Gamma_i^{T,eq}, \quad (35a)$$

$$O(\varepsilon^1) : (\mathbf{I} \partial_{t1} + \mathbf{E}_x \partial_{x1} + \mathbf{E}_y \partial_{y1}) \Gamma_i^{T,(0)} = -\frac{1}{\Delta t} \mathbf{N}_{\mathbf{T}}^{-1} \mathbf{S}_{\mathbf{T}} \mathbf{N}_{\mathbf{T}} \Gamma_i^{T,(1)}, \quad (35b)$$

$$O(\varepsilon^2) : \partial_{t2} \Gamma_i^{T,(0)} + (\mathbf{I} \partial_{t1} + \mathbf{E}_x \partial_{x1} + \mathbf{E}_y \partial_{y1}) (\mathbf{I} - \frac{1}{2} \mathbf{N}_{\mathbf{T}}^{-1} \mathbf{S}_{\mathbf{T}} \mathbf{N}_{\mathbf{T}}) \Gamma_i^{T,(1)} = -\frac{1}{\Delta t} \mathbf{N}_{\mathbf{T}}^{-1} \mathbf{S}_{\mathbf{T}} \mathbf{N}_{\mathbf{T}} \Gamma_i^{T,(2)}, \quad (35c)$$

where $\mathbf{E}_i = \mathbf{M}_{\mathbf{T}} [\text{diag}(e_{0i}, e_{1i}, \dots, e_{4i})] \mathbf{M}_{\mathbf{T}}^{-1}$ ($i = x, y$) can be written explicitly as

$$\mathbf{E}_x = \begin{bmatrix} 0 & 1 & 0 & 0 & 0 \\ 0 & 0 & 0 & 1 & 0 \\ 0 & 0 & 0 & 0 & 0 \\ 0 & 1 & 0 & 0 & 0 \\ 0 & 0 & 0 & 0 & 0 \end{bmatrix}, \quad (36a)$$

$$\mathbf{E}_y = \begin{bmatrix} 0 & 0 & 1 & 0 & 0 \\ 0 & 0 & 0 & 0 & 0 \\ 0 & 0 & 0 & 0 & 1 \\ 0 & 0 & 0 & 0 & 0 \\ 0 & 0 & 1 & 0 & 0 \end{bmatrix}. \quad (36b)$$

Writting out the equations for the conserved raw moment Γ_0^T , the following equations can be obtained,

$$O(\varepsilon^0) : \Gamma_0^{T,(0)} = \Gamma_0^{T,eq}, \quad (37a)$$

$$O(\varepsilon^1) : \partial_{t1}\Gamma_0^{T,(0)} + \partial_{x1}\Gamma_1^{T,(0)} + \partial_{y1}\Gamma_2^{T,(0)} = -\frac{\lambda_0}{\Delta t}\Gamma_0^{T,(1)}, \quad (37b)$$

$$O(\varepsilon^2) : \partial_{t2}\Gamma_0^{T,(0)} + \partial_{t1} \left[\left(1 - \frac{\lambda_0}{2}\right)\Gamma_0^{T,(1)} \right] + \partial_{x1} \left[\left(1 - \frac{\lambda_1}{2}\right)\Gamma_1^{T,(1)} \right] + \partial_{y1} \left[\left(1 - \frac{\lambda_1}{2}\right)\Gamma_2^{T,(1)} \right] = -\frac{\lambda_0}{\Delta t}\Gamma_0^{T,(2)}. \quad (37c)$$

According to Eq. (37a), we have $\Gamma_0^{T,(n)} = 0(n > 0)$. From Eq. (35b), we can get,

$$\Gamma_1^{T,(1)} = -\frac{\Delta t}{\lambda_1} [\partial_{t1}(Tu_x) + \partial_{x1}(Tc_{T,s}^2 + Tu_x^2)], \quad (38a)$$

$$\Gamma_2^{T,(1)} = -\frac{\Delta t}{\lambda_1} [\partial_{t1}(Tu_y) + \partial_{y1}(Tc_{T,s}^2 + Tu_y^2)]. \quad (38b)$$

Substituting Eqs.(38) into Eq.(37a), we can get

$$O(\varepsilon^2) : \partial_{t2}T - \nabla_1 \left[\Delta t \begin{pmatrix} 1/\lambda_1 - 0.5, 0 \\ 0, 1/\lambda_1 - 0.5 \end{pmatrix} \begin{pmatrix} \partial_{t1}(Tu_x) + \partial_{x1}(Tc_{T,s}^2 + Tu_x^2) \\ \partial_{t1}(Tu_y) + \partial_{y1}(Tc_{T,s}^2 + Tu_y^2) \end{pmatrix} \right] = 0. \quad (39)$$

Combining Eq.(37b) with Eq.(39) and Eq.(1a), we can obtain

$$\partial_t T + \mathbf{u} \cdot \nabla T = \nabla \cdot (\alpha \nabla T), \quad (40)$$

where $\alpha = (1/\lambda_1 - 0.5)c_{T,s}^2\Delta t$ is the thermal diffusion coefficient.

References

References

- [1] Y. Qian, D. d'Humières, P. Lallemand, Lattice bkg models for navier-stokes equation, EPL (Europhysics Letters) 17 (6) (1992) 479.
- [2] Y.-H. Qian, S. Succi, S. Orszag, Recent advances in lattice boltzmann computing, Annu. Rev. Comput. Phys 3 (1995) 195–242.
- [3] S. Chen, G. D. Doolen, Lattice boltzmann method for fluid flows, Annual review of fluid mechanics 30 (1) (1998) 329–364.
- [4] S. Succi, The lattice Boltzmann equation: for fluid dynamics and beyond, Oxford university press, 2001.
- [5] S. Gong, P. Cheng, A lattice boltzmann method for simulation of liquid–vapor phase-change heat transfer, International Journal of Heat and Mass Transfer 55 (17-18) (2012) 4923–4927.
- [6] Q. Li, Q. J. Kang, M. M. Francois, Y. L. He, K. H. Luo, Lattice boltzmann modeling of boiling heat transfer: The boiling curve and the effects of wettability, International Journal of Heat and Mass Transfer 85 (2015) 787–796.
- [7] Q. Li, K. Luo, Q. Kang, Y. He, Q. Chen, Q. Liu, Lattice boltzmann methods for multiphase flow and phase-change heat transfer, Progress in Energy and Combustion Science 52 (2016) 62–105.
- [8] S. Chen, B. Yang, K. H. Luo, X. Xiong, C. Zheng, Double diffusion natural convection in a square cavity filled with nanofluid, International Journal of Heat and Mass Transfer 95 (2016) 1070–1083.
- [9] W. Gong, S. Chen, Y. Yan, A thermal immiscible multiphase flow simulation by lattice boltzmann method, International Communications in Heat and Mass Transfer (2017) In press.
- [10] I. Ginzburg, D. d'Humières, Multireflection boundary conditions for lattice boltzmann models, Physical Review E 68 (6) (2003) 066614.
- [11] C. Pan, L.-S. Luo, C. T. Miller, An evaluation of lattice boltzmann schemes for porous medium flow simulation, Computers & fluids 35 (8) (2006) 898–909.
- [12] Z. Guo, C. Zheng, Analysis of lattice boltzmann equation for microscale gas flows: relaxation times, boundary conditions and the knudsen layer, International Journal of Computational Fluid Dynamics 22 (7) (2008) 465–473.

- 170 [13] P. Lallemand, L.-S. Luo, Theory of the lattice boltzmann method: Dispersion, dissipation, isotropy, galilean invariance, and stability, *Physical Review E* 61 (6) (2000) 6546.
- [14] D. d’Humières, Generalized lattice-boltzmann equations, *Rarefied gas dynamics- Theory and simulations* (1994) 450–458.
- [15] I. Karlin, A. Ferrante, H. Öttinger, Perfect entropy functions of the lattice boltzmann method, *EPL (Europhysics Letters)* 47 (2) (1999) 182.
- [16] S. Ansumali, I. V. Karlin, Stabilization of the lattice boltzmann method by the h theorem: A numerical test, *Physical Review E* 62 (6) (2000) 7999.
- [17] S. Ansumali, I. V. Karlin, H. C. Öttinger, Minimal entropic kinetic models for hydrodynamics, *EPL (Europhysics Letters)* 63 (6) (2003) 798.
- 180 [18] I. Ginzburg, Equilibrium-type and link-type lattice boltzmann models for generic advection and anisotropic-dispersion equation, *Advances in Water resources* 28 (11) (2005) 1171–1195.
- [19] I. Ginzburg, F. Verhaeghe, D. d’Humières, Two-relaxation-time lattice boltzmann scheme: About parametrization, velocity, pressure and mixed boundary conditions, *Communications in computational physics* 3 (2) (2008) 427–478.
- [20] M. Geier, A. Greiner, J. G. Korvink, Cascaded digital lattice boltzmann automata for high reynolds number flow, *Physical Review E* 73 (6) (2006) 066705.
- [21] X. Shan, H. Chen, Lattice boltzmann model for simulating flows with multiple phases and components, *Physical Review E* 47 (3) (1993) 1815.
- [22] D. Lycett-Brown, K. H. Luo, Multiphase cascaded lattice boltzmann method, *Computers & Mathematics with Applications* 67 (2) (2014) 350–362.
- 190 [23] D. Lycett-Brown, K. H. Luo, R. Liu, P. Lv, Binary droplet collision simulations by a multiphase cascaded lattice boltzmann method, *Physics of Fluids* 26 (2) (2014) 023303.
- [24] D. Lycett-Brown, K. H. Luo, Improved forcing scheme in pseudopotential lattice boltzmann methods for multiphase flow at arbitrarily high density ratios, *Physical Review E* 91 (2) (2015) 023305.
- [25] D. Lycett-Brown, K. H. Luo, Cascaded lattice boltzmann method with improved forcing scheme for large-density-ratio multiphase flow at high reynolds and weber numbers, *Physical Review E* 94 (5) (2016) 053313.
- [26] L. Fei, K. Luo, Thermal cascaded lattice boltzmann method, *arXiv preprint arXiv:1610.07114*.
- [27] X. Shan, Simulation of rayleigh-bénard convection using a lattice boltzmann method, *Physical Review E* 55 (3) (1997) 2780.
- [28] X. He, S. Chen, G. D. Doolen, A novel thermal model for the lattice boltzmann method in incompressible limit, *Journal of Computational Physics* 146 (1) (1998) 282–300.
- 200 [29] Z. Guo, B. Shi, C. Zheng, A coupled lattice bgk model for the boussinesq equations, *International Journal for Numerical Methods in Fluids* 39 (4) (2002) 325–342.
- [30] Q. Li, Y. He, Y. Wang, G. Tang, An improved thermal lattice boltzmann model for flows without viscous heat dissipation and compression work, *International Journal of Modern Physics C* 19 (01) (2008) 125–150.
- [31] Y. Wang, Y. L. He, Q. Li, G. H. Tang, Numerical simulations of gas resonant oscillations in a closed tube using lattice boltzmann method, *International Journal of Heat and Mass Transfer* 51 (11) (2008) 3082–3090.
- [32] S. Gong, P. Cheng, Lattice boltzmann simulation of periodic bubble nucleation, growth and departure from a heated surface in pool boiling, *International Journal of Heat and Mass Transfer* 64 (3) (2013) 122–132.
- [33] B. Yang, S. Chen, C. Cao, Z. Liu, C. Zheng, Lattice boltzmann simulation of two cold particles settling in newtonian fluid with thermal convection, *International Journal of Heat and Mass Transfer* 93 (2016) 477–490.
- 210 [34] A. Mezrhab, M. A. Moussaoui, M. Jami, H. Naji, M. Bouzidi, Double mrt thermal lattice boltzmann method for simulating convective flows, *Physics Letters A* 374 (34) (2010) 3499–3507.
- [35] J. Wang, D. Wang, P. Lallemand, L.-S. Luo, Lattice boltzmann simulations of thermal convective flows in two dimensions, *Computers & Mathematics with Applications* 65 (2) (2013) 262–286.
- [36] Q. Liu, Y.-L. He, D. Li, Q. Li, Non-orthogonal multiple-relaxation-time lattice boltzmann method for incompressible thermal flows, *International Journal of Heat and Mass Transfer* 102 (2016) 1334–1344.
- [37] S. Cui, N. Hong, B. Shi, Z. Chai, Discrete effect on the halfway bounce-back boundary condition of multiple-relaxation-time lattice boltzmann model for convection-diffusion equations, *Physical Review E* 93 (4) (2016) 043311.
- [38] L. Fei, K. Luo, Consistent forcing scheme in the cascaded lattice boltzmann method, *arXiv preprint arXiv:1705.11092v2*.
- 220 [39] K. N. Premnath, S. Banerjee, Incorporating forcing terms in cascaded lattice boltzmann approach by method of central moments, *Physical Review E* 80 (3) (2009) 036702.
- [40] P. Asinari, Generalized local equilibrium in the cascaded lattice boltzmann method, *Phys Rev E* 78 (2) (2008) 016701.
- [41] Q. Zou, X. He, On pressure and velocity boundary conditions for the lattice boltzmann bgk model, *Physics of fluids* 9 (6) (1997) 1591–1598.
- [42] Z. Guo, C. Zheng, B. Shi, T. Zhao, Thermal lattice boltzmann equation for low mach number flows: decoupling model, *Physical Review E* 75 (3) (2007) 036704.
- [43] D. R. Noble, S. Chen, J. G. Georgiadis, R. O. Buckius, A consistent hydrodynamic boundary condition for the lattice boltzmann method, *Physics of Fluids* 7 (1) (1995) 203–209.
- [44] R. Clever, F. Busse, Transition to time-dependent convection, *Journal of Fluid Mechanics* 65 (04) (1974) 625–645.
- 230 [45] N. I. Prasianakis, I. V. Karlin, Lattice boltzmann method for thermal flow simulation on standard lattices, *Physical Review E* 76 (1) (2007) 016702.